NANO LETTERS

Letter

pubs.acs.org/NanoLett

Size-Selected Monodisperse Nanoclusters on Supported Graphene: Bonding, Isomerism, and Mobility

Bo Wang,[†] Bokwon Yoon,[‡] Michael König,[†] Yves Fukamori,[†] Friedrich Esch,*[,†] Ueli Heiz,[†] and Uzi Landman[‡]

[†]Chemistry Department, Technische Universität München, 85748 Garching, Germany

[‡]School of Physics, Georgia Institute of Technology, Atlanta, Georgia 30332, United States

Supporting Information

ABSTRACT: Soft-landing of size-selected Pd_n ($n \leq 20$) nanoclusters on a Moiré-patterned surface of graphene adsorbed on Ru(0001) leads to controlled formation of a truly monodisperse cluster-assembled material. Combined scanning tunneling microscopy and first-principles calculations allow identification of selective adsorption sites, characterization of size-dependent cluster isomers, and exploration of interconversion processes between isomeric forms that manifestly influence cluster surface mobility. Surface-assembled cluster superstructures may be employed in nanocatalytic applications, as well as in fundamental investigations of physical factors controlling bonding, structure, isomerism, and surface mobilities of surface-supported clusters.

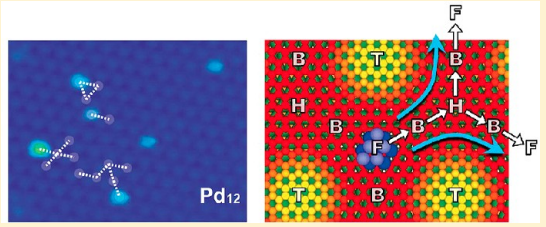

KEYWORDS: *Size-selected supported Pd clusters, epitaxial graphene Moiré substrate, selective adsorption, isomerism-guided diffusion, STM, first-principles DFT calculations*

The use of cluster materials in various fields, ranging from optics and electronics to catalysis, brings new opportunities and expands our ability to design and control materials' functionalities on the atomic scale, owing to the unique chemical and physical properties of these nanostructures.[1] The unique properties of materials' aggregates with nanoscale dimensions often originate from quantum size effects that emerge at reduced sizes, thus introducing size (or scale) as an added dimension to the periodic table of the elements.[1,2] The emerging opportunity of rational design of nanostructured functional materials is based on a deeper understanding of the interplay between morphology and electronic structure as a function of the cluster size. To make progress toward this aim necessitates the development of a methodology that allows a refined degree of monodispersity, a term that we use here in a broadened sense to include not only an absolutely precise selection of particle size but also an ultrasharp distribution of isomeric form and adsorption (support) environment.[3]

We undertake the challenge of preparing materials with the aforementioned unique characteristics via soft-landing size-selected clusters on a long-range-ordered substrate that exhibits a well-defined superstructure and serves as a template, guiding the impinging clusters to spatially separated and highly specific adsorption sites. Catalytically grown graphene films on late transition metal substrates, such as Ru (denoted in the following as g/Ru(0001)), exhibit an extended Moiré pattern with periodicities of about 3 nm and terrace widths of up to 1 μm and prove to be most appropriate for our purpose.[4,5] The formation of nanoscale particles on such surfaces has been the topic of extensive studies that contributed considerably to our general understanding of the adsorption behavior.[6−10] However, several limitations have been encountered in such investigations. First, atomic vapor deposition (AVD), employed as a cluster growth method in earlier studies, precludes size selection[6] and hence does not allow a direct comparison between experiment and theory,[11] as well as inhibits investigation of isomerism. Second, with the AVD preparation, cluster coverages and sizes could not be independently tuned, thus precluding systematic investigations of cluster properties (e.g., structure, isomerism, mobility, and chemical reactivity) as a function of particle size and adsorption environment. As elaborated in the following, the above shortcomings are overcome in the present study that focuses on size-selected Pd clusters soft-landed on the Moiré pattern of the g/Ru(0001) surface. Soft-landing requires kinetic energies per landing cluster atom that are sufficiently smaller than typical binding energies in the cluster; as a rule-of-thumb, soft-landing is commonly achieved for landing energies <1 eV/atom.[1]

Typical cluster distributions obtained by soft-landing of Pd_{19} and Pd_{20} clusters on g/Ru(0001) are depicted in Figure 1a,b, respectively. A homogeneous distribution is observed with no aggregation at steps in striking contrast to the heavy aggregation of Pd clusters grown via AVD.[8] The successful soft-landing of the clusters, that is, without fragmentation, is deduced directly from the absence of small single-layer fragments or defects in the graphene film.[12] However, when the kinetic energy of the clusters is purposefully increased, small

Received: September 6, 2012
Revised: October 11, 2012
Published: October 11, 2012

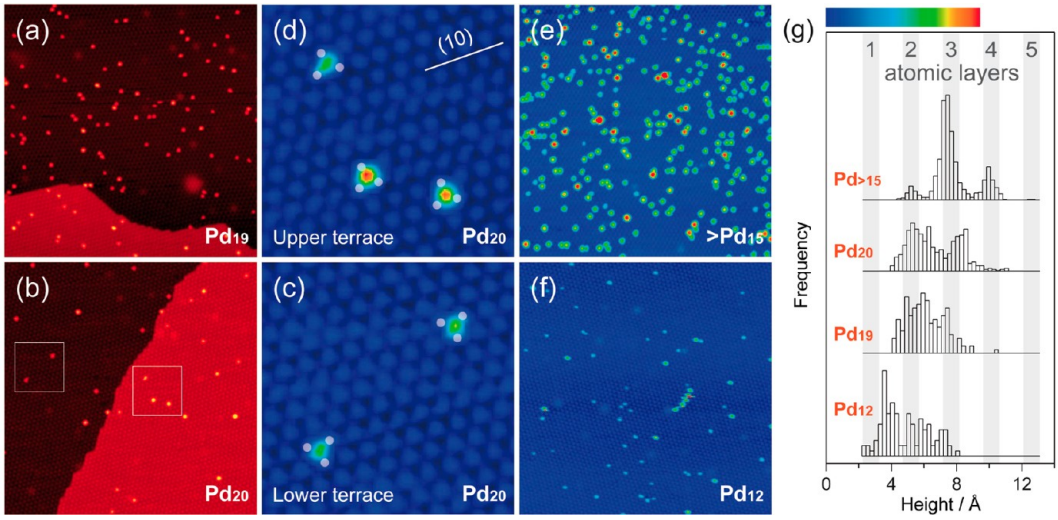

Figure 1. Homogeneous cluster distribution and single adsorption site. Large-scale STM images of Pd clusters soft-landed on g/Ru(0001) at RT: (a) Pd_{19}, (b) Pd_{20} (with indicated areas enlarged in (c) and (d)), (e) size-distributed $Pd_{>15}$, and (f) Pd_{12} clusters. All distributions are homogeneous and show no aggregation at steps. Dots in (c) and (d) denote the nearest T registries (see text) around each cluster; the 180° rotation from one terrace to the next indicates the same F registries. (g) Corresponding height histograms, normalized to relative frequencies. Distinct layer peaks can be resolved. Only for the smallest observed cluster size, Pd_{12}, one-layer clusters are observed; the three-layer peak is assigned to coalescence of two-layer isomers, the most mobile species observed in this study. Image sizes, 165 × 165 nm^2 (a,b, e,f), respectively 32 × 32 nm^2 (c,d); imaging conditions, +1 V, 100 pA. The images taken on a single terrace are displayed with the color scale indicated in (g).

mobile fragments and surface defects do appear (see Supporting Information).

A closer examination of the deposited clusters, shown in Figures 1c,d for Pd_{20}, reveals that adsorption occurs at a highly specific adsorption site (for illustrations of the various cluster adsorption sites on the Moiré-pattern of the metal−supported graphene film, see Figure S1 in the Supporting Information). As a reference for the site assignment we use the well-resolved substrate protrusions,[13] where graphene carbon rings are centered on top of a Ru atom; the so-called ring-top sites (T)[14] where the graphene-metal interaction is smallest. Three T features surround each cluster symmetrically and the so-formed triangles have the same orientation on each terrace but are rotated by 180° on neighboring terraces. This alternating orientation is characteristic to hexagonal close-packed crystals such as Ru and it is a manifestation of the fact that on both terraces the clusters are adsorbed at identical ring-hollow sites. A closer analysis in the vicinity of graphene steps[15] leads unequivocally to a ring-fcc (fcc) (F) adsorption-site assignment, where a carbon ring is centered on a fcc site of the Ru(0001) surface. This site specificity is generic, applying also to larger size-distributed clusters (see Figure 1e for Pd_n, $n > 15$), as well as for size-selected Pd_{12} clusters (Figure 1f) and illustrates the sensitivity of the clusters' binding energy to interactions with atoms as distant as the second underlying metal layer.

Since the graphene film is well ordered over length scales of up to 1 μm, reliable information can be obtained not only on individual clusters but also pertaining to statistics over hundreds of clusters. The histogram of a sample with Pd_n, $n > 15$, shown in Figure 1g exhibits distinct peaks corresponding to clusters having different numbers of atomic layers. The interlayer spacings are found to be about 2.5 Å, halfway between the step height of Pd(111) (2.2 Å) and the typical Pd−Pd bond length in the bulk (2.7 Å). Remarkably, no single-layer peak is observed, indicating reliable size selection and true soft-landing conditions. Notably, the height histogram is found to be sensitive to the cluster size, as illustrated by a comparison of the Pd_{19} and Pd_{20} samples; three-layer isomers are more pronounced for Pd_{20} than for Pd_{19}. The absence of single-layer isomers implies that the Pd_{19}/Pd_{20} clusters maintain a three-dimensional (3D) structure comparable to that in the gas phase[16,17] and avoid wetting of the substrate.[18,19] The cluster−substrate interaction remains thus rather weak with respect to the stronger Pd−Pd binding.

Even for a perfectly size-selected cluster deposition process, Poisson statistics predict formation of a minor amount of dimer clusters. Consequently, for the coverages used in this work (<5% clusters/Moiré cell), we expect a <2.4% dimer fraction,[6,20] assuming that the clusters are immobile at the deposition temperature. This is indeed the case for Pd_{19} and Pd_{20} clusters at room temperature (RT) and we attribute the very small fraction of four-layer clusters in the respective images to such dimers. For small clusters, for example, Pd_{12} (Figure 1f), where we expect, instead, a height of one or two layers, the appearance of a considerable fraction of three-layer clusters is assigned to cluster mobility that leads to coalescence. This mobility is reflected in the streaky appearance of the Pd_{12} clusters in general, and is occasionally observed in diffusion traces as cluster chains (Figures 1f and 2f) caused by displacement of clusters in front of the tip. While it may be possible that the tip facilitates certain elementary cluster diffusion steps, we note that the cluster height distributions do not change significantly upon repeated scanning over the same area. This allows us to conclude that the recorded height distributions portray the intrinsic relative stabilities of the clusters, reflecting the isomer distributions for each cluster size.

A primary manifestation of isomerism is the occurrence of interconversions between different isomers, as presented in Figure 2a,b for Pd_{20}. The two subsequent STM images are part of a sequence acquired during a 30 min interval. Cluster isomerization from a three-layer to a two-layer structure can be recognized in the images and the corresponding line-profiles. This process is not time-reversible, suggesting that the two-layer isomers are energetically more stable than the three-layer

dx.doi.org/10.1021/nl303319f | Nano Lett. 2012, 12, 5907−5912

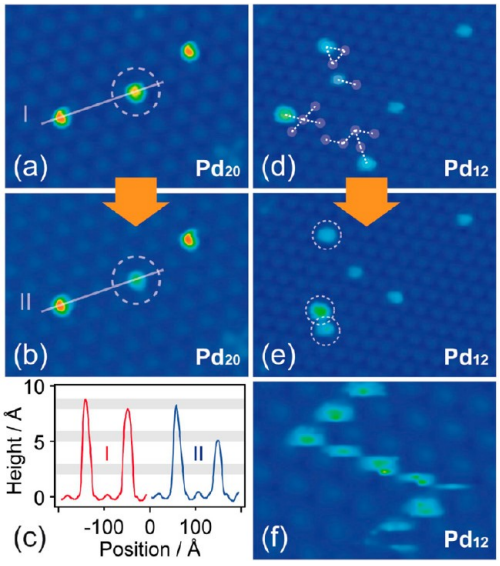

Figure 2. Cluster isomerism and its influence on the cluster mobility. (a,b) Subsequent STM images of Pd_{20} clusters in a time series over 30 min (Δt = 1 min) reveal a cluster isomerization event with an irreversible height change from three- to two-layer, as indicated in the height profiles in (c), taken along line I (in a) and II (in b). (d,e) Isomer-dependent diffusion of Pd_{12} clusters under scanning conditions at RT in a time series over 20 min (Δt = 1 min). All observed trajectories are indicated in (d). They have no preferential direction and are thus not dictated by the scanning direction, even if a tip-induced enhancement of the diffusion cannot be excluded. The two-layer isomers, that is, those with smaller footprint, show higher mobility. Pd_{12} clusters can be manipulated by a strongly interacting STM tip, that is, with a small tip−sample distance, leading to a path that connects F sites, as seen in (f); note that the slow scanning direction is from bottom to top. Image sizes, 30 × 21 nm^2 (a,b), respectively 41 × 31 nm^2 (d,e) and 19 × 14 nm^2 (f); imaging conditions, +1 V, 100 pA. Color scale indicated in Figure 1g.

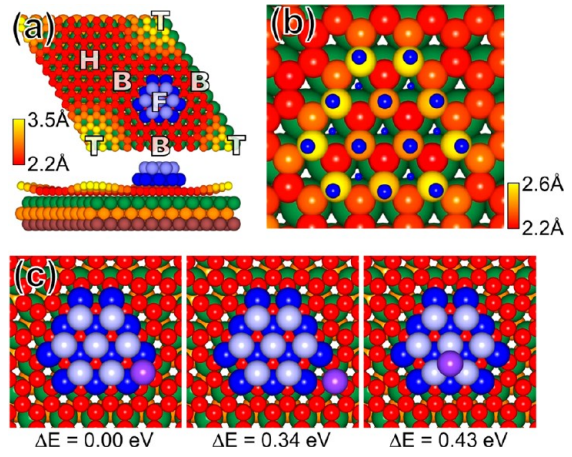

Figure 3. Cluster trapping sites and structure of Pd_{19} and Pd_{20} clusters as obtained by DFT calculations. (a) Top (up) and side (bottom) views of the lowest-energy two-layer Pd_{19} cluster isomer adsorbed at the favorable F-site of the Moiré unit cell of the g/Ru(0001) surface (modeled by three metal layers) with other distinct adsorption sites indicated as H, B, and T (for adsorption energies see Table 1). The heights of the carbon atoms from the topmost layer of the Ru(0001) surface are color coded (see scale at the left). The underlying Ru atoms are depicted as green spheres. (b) Height variations of graphene carbon atoms (with the height-color scale shown on the right) underneath (and in the peripheral vicinity) of the Pd_{19} cluster footprint. The 12-atom bottom layer of the Pd cluster is represented by larger blue spheres, and the second layer is depicted by smaller blue spheres. (c) The lowest energy Pd_{20} isomers with the total energies given in reference to the isomer on the left whose total energy is taken as the zero of the energy scale. These configurations were obtained starting from the lowest energy Pd_{19} adsorbed isomer with the added atom bound in several optional ways. The three-layer cluster isomer (right-hand configuration) is the least stable.

ones (in agreement with our theoretical calculations). In contrast, free Pd_{20} clusters prefer to adopt a 3D structure with three or four layers and this is likely the reason that initially a large fraction of the deposited clusters is found to be three layers high. The first-principles simulations indicate that structural rearrangement can occur without a significant change of the lateral appearance (footprint) of the cluster (see Figure 3c below). Generally speaking, caution should be exercised deducing cluster shapes from STM measurements alone (particularly pertaining to the lateral cluster dimension), since the cluster shape is convoluted with that of a tip whose size is comparable to that of the cluster. Therefore, taller clusters map larger tip circumferences and consequently they often appear larger in the STM images than they really are (see the single-layer and two-layer Pd_{12} clusters imaged in Figure 2d,e).

While Pd_{20} isomers do not appear to diffuse at RT, this changes drastically for smaller clusters; see Figures 2d,e for Pd_{12}. In these images, two types of isomers, one with single layer height and the other two-layer high, can be identified. Their RT mobilities have been investigated in a time series, taken under the same conditions as for the Pd_{20} clusters. It is apparent that the cluster mobility correlates with the height of the cluster with the measurement recording, almost exclusively, mobility of only the two-layer isomer. This is indicated by the diffusion traces drawn in Figure 2d. Since the number of atoms in each of these isomers is the same, the two-layer clusters have a smaller footprint, that is, less atoms in direct contact with the substrate. This appears to be the control parameter that governs the different dynamic properties of the isomers. A 12-atom footprint stabilizes the clusters sufficiently, anchoring them to the substrate and turning them effectively immobile at RT, at least on a time scale of 30 min. This leads us to anticipate that larger clusters, for example, Pd_{19} and Pd_{20}, that are also found to be immobile at RT, should have similar (at least 12 atom) footprints.

The footprints of the adsorbed Pd_n (n = 12, 19, 20) clusters have been determined by an extensive analysis of theoretical calculations with the corresponding energies summarized (for n = 12 and 19) in Table 1. Both Pd_{19} and Pd_{20} are characterized by stable isomers that contain twelve atom footprints (for Pd_{19} see Figure 3a,b and for Pd_{20} see Figure 3c). The most stable isomer found for Pd_{19} is two-layer high, and a similar structure with an added extra atom is found for the Pd_{20} cluster. For the latter, the most stable isomer has a two-layer structure (Figure 3c, left) with the added atom located in the second layer and coordinated to four Pd atoms. In a second isomer (Figure 3c, middle), with an increased total energy of 0.34 eV, the additional atom is adsorbed at a corner of the cluster on the graphene layer and coordinates to two Pd atoms. Finally, a three-layer isomer is found (Figure 3c, right) with the added atom coordinated to three Pd atoms, yielding a total energy that is 0.43 eV higher with respect to the most stable isomer. This result is in line with the experimental observations since the isomerization from a three- to two-layer Pd_{20} isomer is energetically favorable. Furthermore, calculations for Pd_{12}

dx.doi.org/10.1021/nl303319f | Nano Lett. 2012, 12, 5907−5912

Table 1. Calculated Total Energies for the Most Stable Isomer of Pd_{12} and Pd_{19}[a]

	total energies relative to the F site	
binding site	Pd_{12}	Pd_{19}
F	0.00 (5.22, 4.91)	0.00 (6.27, 5.87)
H	0.48	0.86
B	1.00	1.28
T	1.89	3.32

[a]The values (in eV units) are referenced to the binding at the most stable site (F). In parentheses, the absolute binding energies are given as obtained from the total energies, as $[E(g/Ru) + E(Pd_n)] - E(Pd_n/g/Ru)$. The first value in parentheses refers to the energy, $E(Pd_n)$, of a free Pd_n cluster with a structure as the one optimized on the surface, and the second value refers to a free Pd_n cluster with an optimized gas-phase structure.

confirm the existence of isomers with different heights but comparable total energy. The most stable isomer has a 3D (two-layer) structure with a 7-atom hexagonally shaped footprint binding to the underlying graphene surface (Figure 4a), and a 5-atom second layer (Figure 4c). The 2D isomer with a 12-atom footprint, instead, has a total energy higher by 1.05 eV.

Interestingly, all cluster structures follow the same sequence of stability on the g/Ru(0001) surface (see Table 1) with the most stable adsorption site being centered on an F site of the graphene Moiré pattern, confirming the experimental observations. Adsorption on an H site is less favorable by at least ~0.5 eV, followed by even less favorable binding to B and T sites. In general, the clusters tend to bind to those sites where the graphene is closest to the metal substrate. This binding is indeed dominated by the footprint, with similar absolute binding energies found for all Pd_n clusters with a footprint of 12 atoms bound to F sites, and scaling, to a good approximation, with the number of atoms in the footprint. This indicates a rather local binding mechanism with bonds of highly covalent character. A closer inspection of the Pd_{19} cluster reveals marked height variations of the graphene atoms in the immediate vicinity of the adsorbed cluster, and especially under the circumference atoms of the footprint (see color-height coding in Figure 3b). Analysis of bond angles and bond lengths reveals formation of strong metal−carbon hybrids, that is, Ru(4d)−$C(2p_z)$ and Pd(4d)−$C(2p_z)$ covalent bonds, similar to earlier findings[9] for g/Ir(111). Carbon atoms under the adsorbed cluster and at the footprint periphery bind, alternatingly, to a Pd adatom above or to a Ru atom below the graphene layer; the circumference carbon atoms are lifted upward by up to 0.3 Å with respect to the pristine Ru-supported graphene film. In this picture, the sp^2 bonding of the graphene film rehybridizes locally to diamond-like sp^3 bonding.[9] In addition, we find that the cluster becomes slightly positively charged ($\Delta Q = -0.32$ e) upon binding to the graphene film and that it gets polarized with the second layer gaining 0.44 e whereas the first layer loses 0.76 e. The Pd clusters are not found to pin the graphene layer to the underlying Ru substrate, unlike the case[9] of Ir clusters

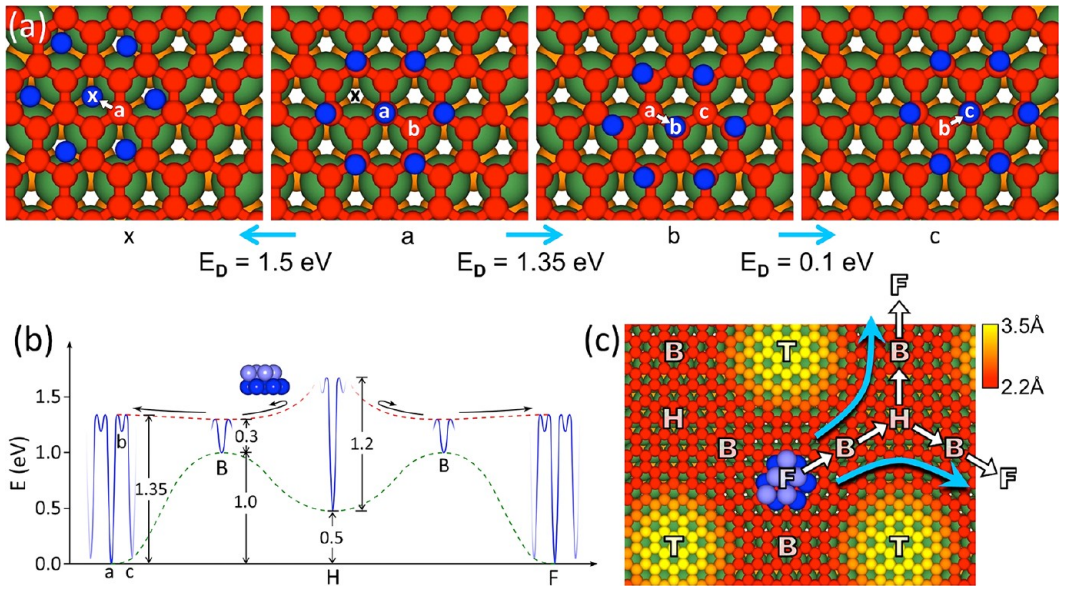

Figure 4. Diffusion path of a mobile, low footprint (two-layer) Pd_{12} isomer. (a) Displacement of the cluster with the center of mass (com) moving along the C−C bond (see a → b) requires a smaller activation energy barrier than motion of the com in the direction of the center of the honeycomb ring (see a → x). In the calculated diffusion path (a → b → c) with the lowest activation barrier, the first step out of the F adsorption site (a → b) requires a much larger activation energy than the subsequent step (b → c). The following diffusion steps (in the direction of the B-site region) require successively smaller activation energies. (b) Schematic energy-surface diagram that summarizes the results of the calculations, displaying the relative values of the binding energies of the cluster to the surface (relative to the F site taken as the zero of the energy scale), the respective calculated outward diffusion barriers from the F, B, and H sites (with a, b, and c marked in the F region, on the left, corresponding to the path a-b-c in panel (a)), and the range of upper and lower bounds for the variation along the diffusion path of the interaction energy of the cluster with the surface. Note the relatively high energy barrier (~0.4 eV) inhibiting diffusion of the cluster into the H region, while the highest local barrier for diffusion out of an adsorption site is found for the F site. These activation barriers lead to almost exclusive population of F sites under the investigated conditions. (c) Part of the Moiré formed by the graphene layer on the Ru(0001) with the two-layer Pd_{12} cluster adsorbed at the F site; the color scale in the upper right gives the distance of the carbon atom from the topmost layer of the underlying metal surface. Superimposed we show most probable diffusion paths (blue arrows) of the cluster between adjacent F sites (see panels (a,b)), constructed from the results of the first-principles calculations.

dx.doi.org/10.1021/nl303319f | Nano Lett. 2012, 12, 5907−5912

supported on graphene/Ir(111). This is because the interaction of the graphene layer with the Ru substrate is stronger than that for an Ir surface, leading to a large corrugation of about 1.0 −1.2 Å in g/Ru(0001) even without the presence of the adsorbed clusters.

Because of the selective binding on the graphene Moiré pattern, the cluster mobility has been commonly correlated with the adsorption strength difference at the high-symmetry sites along the diffusion path.[21] From the STM images, we observe (e.g., Figure 2f) that the clusters diffuse through a bridge (B) site between two F sites. In the following, we distinguish between two diffusion regimes: a local diffusion (LD) one that applies to diffusive transport of a cluster in the immediate neighborhood of the principal adsorption sites (F, H, B, and T), and a global diffusion (GD) mode that refers to mobility of the cluster on the Moiré potential energy surface between (connecting) the local adsorption sites (see Figure 4b,c). As we argue below, the LD barrier plays a dominant role in determining the cluster mobility on the graphene Moiré superstructure. Furthermore, the LD characteristics also underlie our understanding of the manner by which clusters reach the preferred adsorption site (F-site) subsequent to soft-landing deposition on the surface, particularly in light of the relatively large size of the Moiré supercell (~3 nm) compared to the cluster footprint and the rather localized capture-basin of the favored adsorption sites (see Figure 4b,c).

Extensive constrained first-principles (CFP) simulations of the diffusion pathways (see Supporting Information) reveal that the LD barriers for cluster motions along C−C bonds are lower than the one encountered for motion toward the center (x) of the graphene honeycomb ring (see panels "a" and "x" in Figure 4a); this holds also for single adsorbed Pd atoms. Starting from the most stable F adsorption site, the lowest LD barrier calculated for the two-layer Pd_{12} cluster is 1.35 eV (see a → b in Figure 4a). For the larger footprint clusters, the calculated activation energies are substantially higher, for example, by ~1.0 eV in the case of the two-layer Pd_{19}, indicating that under the experimental conditions diffusion of the larger clusters is unlikely. The barrier scales roughly as ~200 meV/(footprint atom), a value that agrees with our calculated LD barrier (≤200 meV) for a single Pd atom. Detailed inspection of the relaxed cluster structures during the diffusion process reveals that they remain almost unaltered, reflecting the higher strength of the Pd−Pd bonds relative to the interaction between Pd atoms and the underlying carbon atoms. Diffusive motion starting from the H adsorption site is also found to entail a rather substantial barrier (1.2 eV), while diffusion out of the B site involves a much lower LD barrier (0.3 eV).

In contrast to the relatively high LD barriers associated with cluster escape from the rather narrow capture-basins of the above-noted specific adsorption sites (in particular F and H), we have found that cluster diffusion on regions of the Moiré that are further away from these sites (e.g., T as well as the intersite (B) regions, see Figure 4b,c) entails significantly smaller LD energy barriers. This finding correlates well with the observation that the Pd clusters coalesce essentially instantaneously at RT on HOPG surfaces, because the carbon film in the T region is rather similar to HOPG or free-standing graphene;[13,14] for early theoretical investigations of the diffusion of metal clusters on perfect and defective graphite surfaces see refs 22 and 23. In the picture that emerges from the above considerations, the Moiré-patterned graphene film appears as a rather "slippery" surface (at T and B regions) characterized by low-cluster diffusion barriers, on which some "sticky" adsorption sites (F and H sites) are located, characterized by high local outward diffusion barriers. Furthermore, the (narrow) "H" sticky site is found to be surrounded by a repelling potential energy ridge that acts as a barrier for inward cluster diffusion to the H site (see Figure 4b). The overall global diffusion path between two neighboring "sticky" F sites will therefore circumvent the H sites, while traversing readily through the intersite potential energy terrain (see Figure 4b,c).

The low LD barriers for cluster mobility in regions B and T, away from the preferred specific binding sites, facilitate cluster exploration, upon landing, of the entire Moiré cell, and eventual binding at the specific, most stable, adsorption site (F and H). Consideration of the relative adsorption energies at these sites (see Table 1 and Figure 4b), leads us to conclude that diffusion into the H sites is energetically unfavorable compared to the F site. This underlies our observation of cluster diffusion traces (obtained upon manipulation at high tunneling currents) with the recorded cluster locations found exclusively to be at F sites (Figure 2f). Indeed, the strong energetic bias toward anchoring clusters at particular sites, in juxtaposition with the energy landscape of the g/Ru(0001) Moiré that favors diffusion into the basins of these specific sites, underlie the feasibility of preparing samples with a very high degree of monodispersity (in the broad sense defined in the introduction) with essentially all the clusters experiencing identical binding environments.

In this paper, we provide the first demonstration of the effects of cluster size and isomerization propensity on the diffusion characteristics of adsorbed clusters. Significant insights into the structure, energetics, bonding, and dynamics of clusters adsorbed on the Moiré pattern of a graphene monolayer supported on Ru(0001) have been gained through joint experiments that employed soft-landed truly monodisperse clusters and first-principle theoretical investigations. Our findings provide the first step in an effort directed at understanding the fundamental physical and chemical properties of these unique systems. These research endeavors aim at future successful utilization of such systems for fundamental research, particularly in the area of nanocatalysis, and in chemical and energy technologies.

Methods. *Experimental Section.* The Pd clusters were produced by a high-frequency laser evaporation cluster source[24] in which a 100 Hz Nd:YAG laser is focused on a rotating metal target, yielding a metal plasma with a temperature up to 10 000 K. The plasma is then thermalized by a He pulse with an initial pressure of about 5 bar and a time width less than 1 ms. Clusters nucleate in the He−metal vapor beam that undergoes a supersonic expansion through a nozzle. Positively charged clusters with a well-defined kinetic energy are then directed by a deflector into a quadrupole mass spectrometer (ABB-Extrel, mass limit 16 000 amu), where the mass selection is carried out. The size-selected clusters are further guided through a 2 mm pinhole lens for improved differential pumping and finally reach the preparation chamber. During deposition, the basic chamber pressure is p(He) = 2×10^{-8} mbar and p(residual gas) = 8×10^{-10} mbar.

The Ru(0001) crystal was cleaned by repeated cycles of Ar^+ sputtering and annealing at 1473 K. The graphene monolayer on Ru(0001) was prepared by exposing the crystal to ethylene (2×10^{-7} mbar) for 3 min at 1220 K. This procedure leads to well-ordered Moiré structures that have been extensively described in the literature.[4,5,25] The sample was cooled down

dx.doi.org/10.1021/nl303319f | Nano Lett. 2012, 12, 5907−5912

to RT before the cluster deposition. The supported Pd_n clusters have been characterized by scanning tunneling microscopy (STM) in an Omicron VT-STM at RT.

Calculations. Calculations were performed using the VASP-DFT package with a plane-wave basis (kinetic energy cutoff of 400 eV), PAW pseudopotentials,[26] and the PW91 generalized gradient approximation (GGA) for the exchange-correlation potential.[27−29] Since the unit cell used here is rather large, we have used in most of our calculations a single *k*-point sampling of the surface Brillouin zone (SBZ) at Γ; we have checked that the results remain essentially the same by employing (3 × 3 × 1) sampling. In optimization of the various structures, convergence was achieved for forces smaller than 0.001 eV/Å. The Ru(0001) substrate surface consisted of three layers with the optimized Ru lattice parameters a = 2.724 Å and c = 4.305 Å, agreeing with the experimental values (a = 2.706 Å and c = 4.28 Å); in structural relaxations the bottom layer of the substrate slab was held fixed. In simulations of the adsorption of Pd_n clusters (n = 12 and 19), the supercell had an (11 × 11) lateral periodicity of the three-layer Ru(0001) slab, a (12 × 12) layer of graphene, and a vacuum region that was taken large enough to ensure no interaction between periodic replicas; for the bare g/Ru(0001) system, the vacuum region was taken as 20.3 Å, and it was 15.9 Å when a two-layer Pd_{19} cluster was adsorbed at the highest adsorption site (T). The relaxed configuration of the (11 × 11) structure exhibited a strong vertical modulation of the epitaxial graphene layer, with the highest C atom lying 3.45 Å above the underlying Ru topmost layer and the lowest-lying C atom located at a distance of 2.27 Å, resulting in a height modulation of 1.18 Å.

■ ASSOCIATED CONTENT

Ⓢ Supporting Information

Adsorption sites on the metal−supported graphene film (Figure S1), experimental details on the cluster landing conditions (soft-landing vs hard-landing as depicted in Figure S2), as well as details on the calculations concerning rehybridization analysis, CFP simulations of the diffusion pathways, and the cluster binding in ring-hollow sites (F, H). This material is available free of charge via the Internet at http://pubs.acs.org.

■ AUTHOR INFORMATION

Corresponding Author

*E-mail: friedrich.esch@tum.de.

Notes

The authors declare no competing financial interest.

■ ACKNOWLEDGMENTS

The experimental work was funded by the Deutsche Forschungsgemeinschaft (DFG) through the ESF-EUROCORES project NOMCIS and in part by a grant from the Air Force Office of Scientific Research. Financial support by the National Research Found Luxembourg (Y.F.) and the Friedrich Ebert-Stiftung (M.K.) is gratefully acknowledged. The work of B.Y. and U.L. was supported by the Office of Basic Energy Sciences of the U.S. Department of Energy under Contract No. FG05-86ER45234, and in part by a grant from the Air Force Office of Scientific Research. Computations were made at the GATECH Center for Computational Materials Science. The manuscript was written through contributions of all authors. All authors have given approval to the final version of the manuscript.

■ REFERENCES

(1) Heiz, U.; Landman, U. *Nanocatalysis*; Springer: Berlin, 2007.
(2) Heiz, U.; Sanchez, A.; Abbet, S.; Schneider, W. D. *J. Am. Chem. Soc.* **1999**, *121*, 3214.
(3) Harding, C.; Habibpour, V.; Kunz, S.; Farnbacher, A. N. S.; Heiz, U.; Yoon, B.; Landman, U. *J. Am. Chem. Soc.* **2009**, *131*, 538.
(4) Wu, M. C.; Xu, Q.; Goodman, D. W. *J. Phys. Chem.* **1994**, *98*, 5104.
(5) de Parga, A. L. V.; Calleja, F.; Borca, B.; Passeggi, M. C. G.; Hinarejos, J. J.; Guinea, F.; Miranda, R. *Phys. Rev. Lett.* **2008**, *100*, 056807.
(6) N'Diaye, A. T.; Bleikamp, S.; Feibelman, P. J.; Michely, T. *Phys. Rev. Lett.* **2006**, *97*, 215501.
(7) N'Diaye, A. T.; Gerber, T.; Busse, C.; Myslivecek, J.; Coraux, J.; Michely, T. *New J. Phys.* **2009**, *11*, 103045.
(8) Zhou, Z. H.; Gao, F.; Goodman, D. W. *Surf. Sci.* **2010**, *604*, 1071.
(9) Feibelman, P. J. *Phys. Rev. B* **2008**, *77*, 165419.
(10) Feibelman, P. J. *Phys. Rev. B* **2009**, *80*, 085412.
(11) Knudsen, J.; Feibelman, P. J.; Gerber, T.; Granas, E.; Schulte, K.; Stratmann, P.; Andersen, J. N.; Michely, T. *Phys. Rev. B* **2012**, *85*, 035407.
(12) Palmer, R. E.; Pratontep, S.; Boyen, H. G. *Nat. Mater.* **2003**, *2*, 443.
(13) Wang, B.; Bocquet, M. L.; Marchini, S.; Gunther, S.; Wintterlin, J. *Phys. Chem. Chem. Phys.* **2008**, *10*, 3530.
(14) Wang, B.; Caffio, M.; Bromley, C.; Fruchtl, H.; Schaub, R. *Acs Nano* **2010**, *4*, 5773.
(15) Donner, K.; Jakob, P. *J. Chem. Phys.* **2009**, *131*, 164701.
(16) Rogan, J.; Garcia, G.; Ramirez, M.; Munoz, V.; Valdivia, J. A.; Andrade, X.; Ramirez, R.; Kiwi, M. *Nanotechnology* **2008**, *19*, 205701.
(17) Zhang, H. L.; Tian, D. X.; Zhao, J. J. *J. Chem. Phys.* **2008**, *129*, 114302.
(18) Schaub, R.; Jodicke, H.; Brunet, F.; Monot, R.; Buttet, J.; Harbich, W. *Phys. Rev. Lett.* **2001**, *86*, 3590.
(19) Bromann, K.; Felix, C.; Brune, H.; Harbich, W.; Monot, R.; Buttet, J.; Kern, K. *Science* **1996**, *274*, 956.
(20) Abbet, S.; Judai, K.; Klinger, L.; Heiz, U. *Pure Appl. Chem.* **2002**, *74*, 1527.
(21) Wang, B.; Bocquet, M. L. *J. Phys. Chem. Lett.* **2011**, *2*, 2341.
(22) Luedtke, W. D.; Landman, U. *Phys. Rev. Lett.* **1999**, *82*, 3835.
(23) Yoon, B.; Luedtke, W. D.; Gao, J. P.; Landman, U. *J. Phys. Chem. B* **2003**, *107*, 5882.
(24) Heiz, U.; Vanolli, F.; Trento, L.; Schneider, W. D. *Rev. Sci. Instrum.* **1997**, *68*, 1986.
(25) Pan, Y.; Zhang, H.; Shi, D.; Sun, J.; Du, S.; Liu, F.; Gao, H.-J. *Adv. Mater.* **2009**, *21*, 2777.
(26) Kresse, G.; Joubert, D. *Phys. Rev. B* **1999**, *59*, 1758.
(27) Perdew, J. P. *Electronic Structure of Solids'91*; Ziesche, P., Eschring, H., Eds.; Akademie: Berlin, 1991.
(28) Perdew, J. P.; Chevary, J. A.; Vosko, S. H.; Jackson, K. A.; Pederson, M. R.; Singh, D. J.; Fiolhais, C. *Phys. Rev. B* **1992**, *46*, 6671.
(29) Perdew, J. P.; Chevary, J. A.; Vosko, S. H.; Jackson, K. A.; Pederson, M. R.; Singh, D. J.; Fiolhais, C. *Phys. Rev. B* **1993**, *48*, 4978.